

Estimation of interval anisotropic attenuation from reflection data

Jyoti Behura¹ and Ilya Tsvankin²

ABSTRACT

Knowledge of interval attenuation can be highly beneficial in reservoir characterization and lithology discrimination. We combine the spectral-ratio method with velocity-independent layer stripping to develop a technique for the estimation of the interval attenuation coefficient from reflection seismic data. The layer-stripping procedure is based on identifying the reflections from the top and bottom of the target layer that share the same ray segments in the overburden. The algorithm is designed for heterogeneous, arbitrarily anisotropic target layers, but the overburden is assumed to be laterally homogeneous with a horizontal symmetry plane. Although no velocity information about the overburden is needed, interpretation of the computed anisotropic attenuation coefficient involves the phase angle in the target layer. Tests on synthetic P-wave data from layered transversely isotropic and orthorhombic media confirm the high accuracy of 2D and 3D versions of the algorithm. We also demonstrate that the interval attenuation estimates are independent of the inhomogeneity angle of the incident and reflected waves.

INTRODUCTION

The attenuation coefficient of subsurface rocks is linked closely to their lithology and physical properties. In particular, attenuation may serve as an indicator of permeability, mobility of fluids, and fluid saturation (e.g., Winkler and Nur, 1982; Batzle et al., 2006; Behura et al., 2007). Laboratory measurements (Hosten et al., 1987; Tao and King, 1990; Prasad and Nur, 2003; Behura et al., 2006) and field studies (Ganley and Kanasewich, 1980; Liu et al., 2007; Maultzsch et al., 2007) indicate that attenuation can be strongly anisotropic (directionally dependent) because of the preferential alignment of fractures, interbedding of thin attenuative layers, and/or nonhydrostatic stress. Furthermore, the symmetry of attenuation anisotropy

may be different from that of velocity anisotropy (Maultzsch et al., 2007; Zhu et al., 2007b). Therefore, measurements of attenuation anisotropy may provide valuable additional information about the properties of anisotropic (e.g., fractured) reservoirs (Liu et al., 2007).

Most existing attenuation estimates from reflection data (e.g., Vasconcelos and Jenner, 2005) are obtained for the whole section above the reflecting interface. Dasgupta and Clark (1998) introduced a technique for estimating interval attenuation from reflection data based on the spectral-ratio method. Their algorithm, however, is restricted to zero-offset reflections and requires knowledge of the source signature.

Here, we present a method for computing the interval attenuation coefficient using an extension of the layer-stripping technique originally introduced by Dewangan and Tsvankin (2006) for reflection traveltimes. Our algorithm reconstructs the offset-dependent and azimuth-dependent interval attenuation in a heterogeneous, arbitrarily anisotropic target layer without knowledge of the velocity and attenuation in the overburden. Synthetic examples for layered VTI (transversely isotropic with a vertical symmetry axis) and orthorhombic media confirm the accuracy of our method and its high potential in the inversion for the interval attenuation-anisotropy parameters.

METHODOLOGY

We consider a pure-mode (PP or SS) reflection in a medium that includes an anisotropic, heterogeneous target layer under a laterally homogeneous overburden with a horizontal symmetry plane (Figure 1). For simplicity, the layer-stripping technique is introduced here in two dimensions, although we also have implemented it for 3D wide-azimuth data (see below). To make wave propagation two-dimensional, the vertical incidence plane has to coincide with a plane of symmetry in all layers including the target. As discussed by Dewangan and Tsvankin (2006), this restriction becomes unnecessary in the 3D extension of the layer-stripping method.

Dewangan and Tsvankin (2006) showed that the exact interval traveltime-offset function in the target layer can be constructed by combining the target event with reflections from the bottom of the

Manuscript received by the Editor 5 March 2009; revised manuscript received 15 May 2009; published online 25 November 2009.

¹Formerly Colorado School of Mines, Center for Wave Phenomena, Department of Geophysics, Golden, Colorado, U.S.A.; currently BP America, Exploration and Production Technology, Houston, Texas, U.S.A. E-mail: jyoti.behura@dix.mines.edu

²Colorado School of Mines, Department of Geophysics, Golden, Colorado, U.S.A. ilya@dix.mines.edu

© 2009 Society of Exploration Geophysicists. All rights reserved.

overburden (Figure 1) using the process of matching traveltime slopes (horizontal slownesses) on common-source and common-receiver gathers. First, a common-receiver gather of the target reflection recorded at point G is used to compute the traveltime slope of the event ABCEG at the source location A. Then the time slope of the overburden reflection is evaluated for a range of receiver locations by forming a common-shot gather at point A. For a certain receiver D, the magnitude of the traveltime slope of the overburden reflection coincides with that of the target event. Note that because the horizontal slowness does not change along any ray propagating in the overburden, the time slopes of the overburden event at the source (A) and receiver (D) locations are identical. Therefore, the raypaths ABCEG and ABD share the same downgoing leg AB. Likewise, it is possible to identify the overburden reflection GEF that shares the upgoing (EG) leg with the target event ABCEG.

Under the assumptions made above, any reflection point at the bottom of the overburden (e.g., points B and E in Figure 1) coincides with the common midpoint for the corresponding source-receiver pair, and the traveltimes along the downgoing and upgoing segments of the reflected ray are equal to each other. Therefore, the interval traveltime in the target layer along the path BCE can be found from

$$t_{BCE} = t_{ABCEG} - \frac{t_{ABD} + t_{GEF}}{2}, \quad (1)$$

where t_{ABCEG} , t_{AB} , and t_{GEF} are the traveltimes along the raypaths ABCEG, ABD, and GEF, respectively. Implementation of the kinematic velocity-independent layer-stripping algorithm is described in more detail in the work of Dewangan and Tsvankin (2006).

Here, we extend this layer-stripping technique to attenuation analysis by applying the spectral-ratio method to a specific combination of the target and overburden events. Because the overburden is laterally homogeneous and has a horizontal symmetry plane, $l_{AB} = l_{BD}$ and $l_{EG} = l_{FE}$, where l_{XY} is the distance along the raypath XY. The ray-theory amplitudes of the target and overburden reflections in the frequency domain can be written as

$$|U_{ABCEG}(\omega)| = S(\omega) \mathcal{G}_{ABCEG} e^{-k_{g,o}^I l_{AB} + l_{EG}} e^{-k_{g,T}^I l_{BC} + l_{CE}}, \quad (2)$$

$$\begin{aligned} |U_{ABD}(\omega)| &= S(\omega) \mathcal{G}_{ABD} e^{-k_{g,o}^I l_{AB} + l_{BD}} \\ &= S(\omega) \mathcal{G}_{ABD} e^{-2k_{g,o}^I l_{AB}}, \end{aligned} \quad (3)$$

and

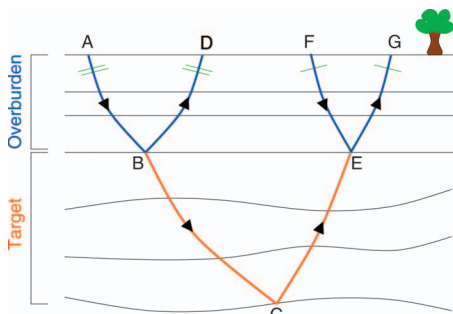


Figure 1. 2D ray diagram of the layer-stripping algorithm. Points B and E are located at the bottom of the overburden. The target reflection ABCEG and the reflection ABD from the bottom of the overburden share the same downgoing leg AB. The upgoing leg EG of the target event coincides with a leg of another overburden reflection GEF.

$$|U_{GEF}(\omega)| = S(\omega) \mathcal{G}_{GEF} e^{-k_{g,o}^I l_{EG} + l_{EF}} = S(\omega) \mathcal{G}_{GEF} e^{-2k_{g,o}^I l_{EG}}, \quad (4)$$

where $k_{g,T}^I$ and $k_{g,o}^I$ (superscript I stands for the imaginary part of the wavenumber) are the average group attenuation coefficients in the target layer and overburden, respectively. $S(\omega)$ is the spectrum of the source wavelet; and the parameters \mathcal{G}_{ABD} , \mathcal{G}_{GEF} , and \mathcal{G}_{ABCEG} include the source-receiver radiation patterns as well as the plane-wave reflection/transmission coefficients and geometric spreading along the corresponding raypaths. The frequency-domain amplitudes of the target and overburden reflections are obtained by windowing the corresponding arrivals and applying the Fourier transform.

To eliminate the contribution of the overburden along with the source wavelet, equations 2, 3, and 4 can be combined in the following way:

$$\ln\left(\frac{|U_{ABCEG}(\omega)|^2}{|U_{ABD}(\omega)||U_{GEF}(\omega)|}\right) = \ln(\mathcal{G}) - 2k_{g,T}^I l_{BC} + l_{CE}, \quad (5)$$

where the term $\mathcal{G} = \mathcal{G}_{ABCEG}^2 / (\mathcal{G}_{ABD} \mathcal{G}_{GEF})$ is assumed to be independent of frequency. Equation 5 can be used to estimate the interval attenuation coefficient in the target layer without knowledge of the source wavelet and overburden parameters.

For an arbitrarily heterogeneous target layer, the attenuation coefficient varies along the ray, and $k_{g,T}^I$ in equation 5 represents the average value along the raypath BCE. However, if the target layer is horizontal, homogeneous, and has a horizontal symmetry plane (or is purely isotropic), then $l_{BC} + l_{CE} = V_g t_{BCE}$, where V_g is the group velocity along the rays BC and CE. Then equation 5 takes the form

$$\ln\left(\frac{|U_{ABCEG}(\omega)|^2}{|U_{ABD}(\omega)||U_{GEF}(\omega)|}\right) = \ln(\mathcal{G}) - 2k_{g,T}^I V_g t_{BCE}. \quad (6)$$

The coefficient $k_{g,T}^I$ generally differs from the phase attenuation coefficient k^I , which can be obtained analytically from the Christoffel equation (e.g., Zhu and Tsvankin, 2006). If the inhomogeneity angle (the angle between the real and imaginary parts of the wave vector; see Figure 2) is zero, the group and phase attenuation coefficients are

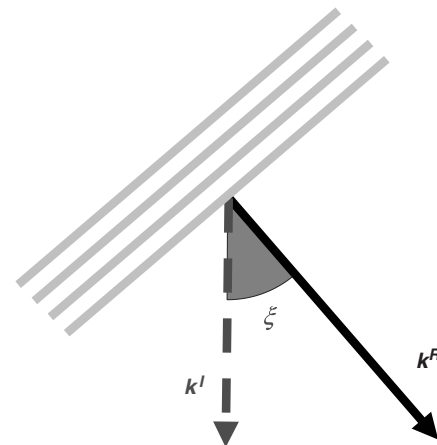


Figure 2. Inhomogeneity angle ξ of a plane wave in attenuative media. k^R and k^I are the real and imaginary components, respectively, of the wave vector.

related by $k_g^I = k^I \cos\psi$, where ψ is the angle between the group- and phase-velocity vectors (Zhu, 2006; Behura and Tsvankin, 2009). Using this relationship and expressing V_g through the phase velocity V ($V_g = V/\cos\psi$), the attenuation-related term in equation 6 can be represented as follows (hereafter, the subscript T is omitted):

$$k_g^I V_g t_{\text{BCE}} = k^I V t_{\text{BCE}} = \omega \frac{k^I}{k^R} t_{\text{BCE}} = \omega \mathcal{A} t_{\text{BCE}}, \quad (7)$$

where $\mathcal{A} = k^I/k^R$ ($k^R = \omega/V$) is the normalized phase attenuation coefficient responsible for the rate of amplitude decay per wavelength (Zhu and Tsvankin, 2006). For isotropic media, $\mathcal{A} = 1/(2Q)$, where Q is the quality factor widely used as a measure of intrinsic attenuation. Substitution of equation 7 into equation 6 yields

$$\ln\left(\frac{|U_{\text{ABCEG}}(\omega)|^2}{|U_{\text{ABD}}(\omega)||U_{\text{GEF}}(\omega)|}\right) = \ln(\mathcal{G}) - 2\omega \mathcal{A} t_{\text{BCE}}. \quad (8)$$

To relate the group and phase attenuation coefficients, we assumed a zero inhomogeneity angle ξ in the target layer (Figure 2). However, as shown by Behura and Tsvankin (2009), equation 8 yields the coefficient $\mathcal{A}|_{\xi=0^\circ}$ (i.e., the intrinsic attenuation) for a wide range of inhomogeneity angles. This result, explained in more detail in the discussion section, is confirmed by the synthetic examples below.

The slope of the logarithmic spectral ratio in equation 8 expressed as a function of ω is equal to the product $2\mathcal{A} t_{\text{BCE}}$. Because the interval traveltime t_{BCE} is obtained from the layer-stripping algorithm (equation 1), application of the spectral-ratio method to the amplitude combination in equation 8 can be used to compute the phase attenuation coefficient \mathcal{A} . In the current analysis, we assume that \mathcal{A} is independent of frequency (i.e., Q is constant), and the slope of the logarithmic spectral ratio does not change within the frequency band of the signal. However, if \mathcal{A} is a function of frequency, then the instantaneous slope would produce a frequency-dependent quality factor. Unless the medium exhibits an anomalously strong velocity dispersion, such as that in heavy oils (Behura et al., 2007), the spectral-ratio method should give reliable attenuation estimates. The potential influence of velocity dispersion can be mitigated by using a reduced frequency range in the spectral-ratio method.

Therefore, our method makes it possible to obtain the normalized phase attenuation coefficient $\mathcal{A} = \mathcal{A}|_{\xi=0^\circ}$ — the quantity dependent on attenuation-anisotropy parameters. The coefficient \mathcal{A} , however, is expressed analytically as a function of the corresponding phase direction (Zhu and Tsvankin, 2006). Hence, inversion of \mathcal{A} for the relevant attenuation-anisotropy parameters requires knowledge of the phase angle for each source-receiver pair. This issue is addressed in more detail in the discussion section.

Computation of the interval values of \mathcal{A} for different source-receiver pairs along the acquisition line can help to evaluate both the in-plane anisotropy and the lateral variation of attenuation. We also extended the methodology described here to wide-azimuth data (see the synthetic example below) using the 3D version of the layer-stripping algorithm presented by Dewangan and Tsvankin (2006) and Wang and Tsvankin (2009). In particular, Wang and Tsvankin (2009) employ the nonhyperbolic moveout equation to develop an efficient implementation of kinematic layer-stripping for wide-azimuth P-wave data from horizontally layered orthorhombic media.

SYNTHETIC EXAMPLES

First we test the method on synthetic P-wave reflection data generated for a horizontally stratified VTI model (Figure 3). Attenuation in VTI media can be characterized conveniently using the Thomsen-style parameters [$\mathcal{A}_{\text{P0}} \approx 1/(2Q_{\text{P0}})$, $\mathcal{A}_{\text{S0}} \approx 1/2(Q_{\text{S0}})$, ϵ_Q , δ_Q , and γ_Q] introduced by Zhu and Tsvankin (2006). \mathcal{A}_{P0} and \mathcal{A}_{S0} are the normalized symmetry-direction attenuation coefficients of P- and S-waves, respectively, ϵ_Q and δ_Q control the angular variation of the P- and SV-wave attenuation coefficients, and γ_Q governs SH-wave attenuation anisotropy.

Figure 4a displays a shot gather computed for the model in Figure 3 by an anisotropic reflectivity code (Schmidt and Tango, 1986). Note that the reflections from the bottom of the attenuative layers have a much lower frequency content than the water-bottom event (Figure 4b). Although the second layer has uncommonly strong attenuation [$\mathcal{A}_{\text{P0}} = 1/(2Q_{\text{P0}}) = 0.05$], the estimated interval attenuation coefficient is close to the exact values for a wide range of propa-


	
Water	$Q = \infty$
VTI	$Q_0 = 10$
VTI	$Q_0 = 200$
VTI half-space	$Q_0 = 100$

Figure 3. Horizontally layered model used to test the 2D attenuation layer-stripping algorithm. The first layer is water (purely elastic and isotropic) with the P-wave velocity $V_p = 1500$ m/s and thickness $d = 1000$ m; the other three layers are VTI. For the second layer, the vertical P- and S-wave velocities are $V_{\text{P0}} = 1600$ m/s and $V_{\text{S0}} = 200$ m/s, $d = 300$ m, and Thomsen velocity-anisotropy parameters are $\epsilon = 0.3$ and $\delta = -0.2$; the attenuation parameters are $Q_{\text{P0}} = 10$, $Q_{\text{S0}} = 10$, $\epsilon_Q = -0.5$, and $\delta_Q = -1.0$. The third layer has $V_{\text{P0}} = 2000$ m/s, $V_{\text{S0}} = 1000$ m/s, $d = 1000$ m, $\epsilon = 0.1$, $\delta = 0.6$, $Q_{\text{P0}} = 200$, $Q_{\text{S0}} = 200$, $\epsilon_Q = -0.3$, and $\delta_Q = 1.0$. For the bottom half-space, $V_{\text{P0}} = 2200$ m/s, $V_{\text{S0}} = 1100$ m/s, $\epsilon = 0$, $\delta = -0.2$, $Q_{\text{P0}} = 100$, $Q_{\text{S0}} = 100$, $\epsilon_Q = 0.5$, and $\delta_Q = 0.5$.

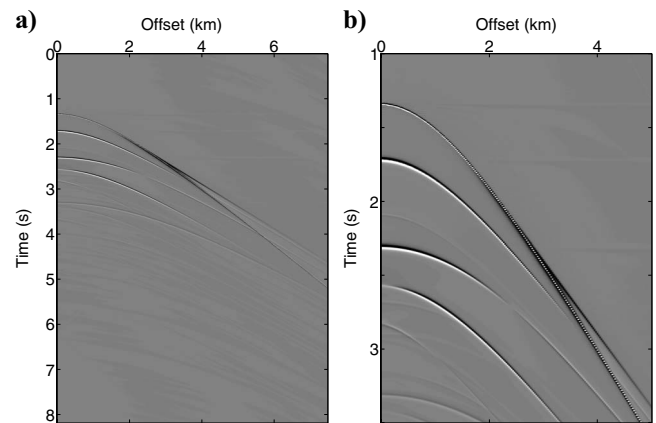


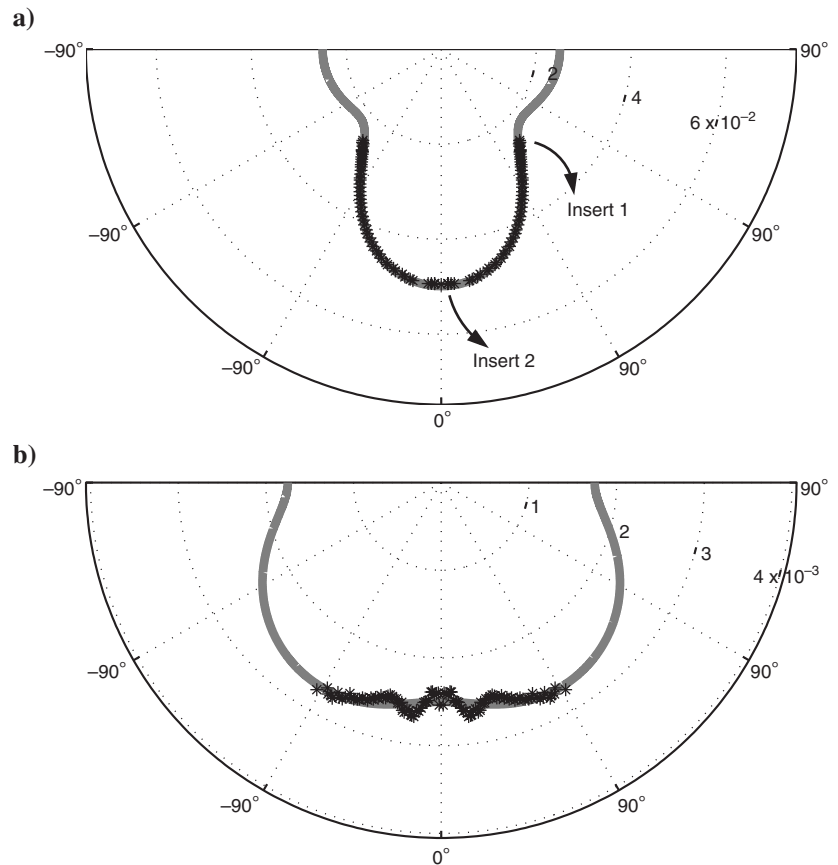
Figure 4. (a) Shot gather computed for the model in Figure 3. (b) A blowup of the gather showing reflections with different frequency content.

gation directions (Figure 5a). Attenuation coefficients for phase angles exceeding 40° are missing because of the limited acquisition aperture. The estimated interval attenuation in the third layer (Figure 5b) is accurate only up to 30° . For larger angles, the target reflection interferes with the direct arrival and other events, which impairs the performance of the spectral-ratio method. Interference-related distortions can be mitigated by operating in the τ - p domain or suppressing the direct arrival and ground roll before layer stripping.

The 3D version of the layer-stripping method was applied to wide-azimuth P-wave data computed for the model in Figure 6. The second and fourth layers exhibit orthorhombic attenuation anisotropy with different azimuths of the vertical symmetry planes, whereas the third layer is VTI. The velocity field is VTI for all the layers except the top one (water). Directionally dependent attenuation coefficients in orthorhombic media can be described using a notation similar to that developed by Tsvankin (1997) for the velocity function. This parameter set includes the P- and S-wave vertical attenuation coefficients (\mathcal{A}_{P0} and \mathcal{A}_{S0}) and seven anisotropy parameters — $\epsilon_Q^{(1,2)}$, $\delta_Q^{(1,2,3)}$, and $\gamma_Q^{(1,2)}$ (Zhu and Tsvankin, 2007).

The estimated interval attenuation coefficient \mathcal{A} in the second (orthorhombic) layer (Figure 7a) practically coincides with the exact \mathcal{A} (Figure 7b) for the whole range of the polar and azimuthal phase angles. The interval attenuation in the third layer (VTI) also is reconstructed with high accuracy (Figure 7c and d). As was the case for the 2D example, the minor difference between the exact and computed attenuation coefficients is caused primarily by interference of the overburden and target reflections with other events.

Figure 5. Normalized interval phase attenuation coefficient \mathcal{A} (stars) estimated as a function of the phase angle (in degrees) for the (a) second and (b) third layers of the model from Figure 3. The solid gray lines mark the exact values of $\mathcal{A}|_{\xi=0^\circ}$. The inhomogeneity angle in the second layer reaches 40° for the largest offset.



DISCUSSION

Although the relationship between the group and phase attenuation coefficients used in our derivation was originally proved for a zero inhomogeneity angle ξ (Figure 2), our method remains accurate for a wide range of ξ . Indeed, as shown by Behura and Tsvankin (2009), the application of equations 6 and 7 for nonzero inhomogeneity angles yields the normalized phase attenuation coefficient \mathcal{A} corresponding to $\xi = 0^\circ$ ($\mathcal{A}|_{\xi=0^\circ}$). This conclusion, which remains valid for large angles ξ up to 80° and media with the quality factor Q as low as 5, is confirmed by the tests shown in Figures 5 and 7. Our algorithm produces accurate values of $\mathcal{A}|_{\xi=0^\circ}$ even for long offsets, where the inhomogeneity angle ξ of the incident and reflected waves reaches 40° .

The coefficient $\mathcal{A}|_{\xi=0^\circ}$ quantifies the intrinsic angle-dependent attenuation of a particular wave mode. For P-waves in transverse isotropy (TI) media, the phase attenuation coefficient linearized in the anisotropy parameters is given by (Zhu and Tsvankin, 2006)

$$\mathcal{A}|_{\xi=0^\circ} = \mathcal{A}_{P0}(1 + \delta_Q \sin^2 \theta \cos^2 \theta + \epsilon_Q \sin^4 \theta), \quad (9)$$

where θ is the phase angle with the symmetry axis. Equation 9 has the same form as the well-known Thomsen's (1986) weak-anisotropy approximation for the P-wave phase-velocity function. Zhu and Tsvankin (2007) present a similar linearized expression for the coefficient $\mathcal{A}|_{\xi=0^\circ}$ of P-waves in attenuative orthorhombic media.

As demonstrated by Zhu et al. (2007a) on physical-modeling data, equation 9 can be used to invert attenuation measurements for the

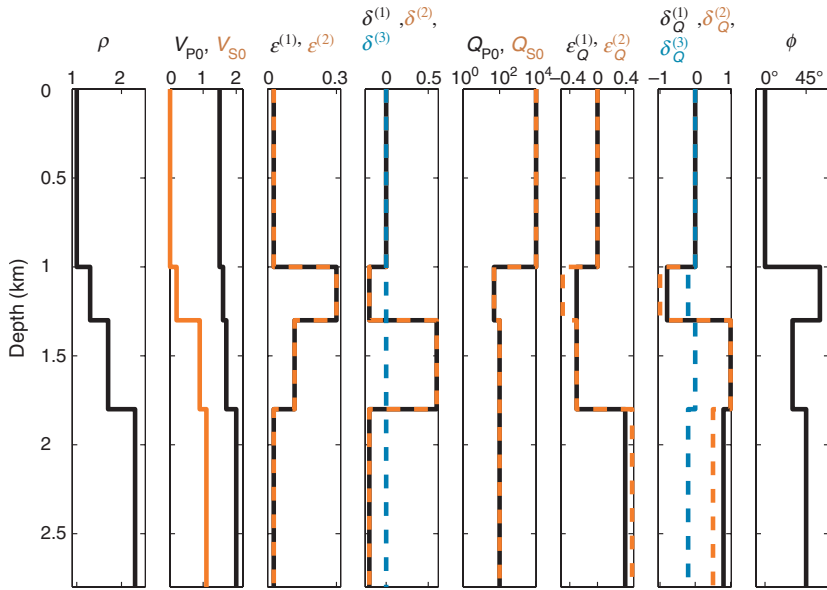


Figure 6. Horizontally layered model used to test the 3D attenuation layer-stripping algorithm. The first layer (top) is isotropic (water), the second and fourth layers have orthorhombic attenuation anisotropy, and the third layer is VTI in terms of attenuation. In terms of velocity, the second to fourth layers are VTI. The velocity and density are in km/s and g/cm³. ϕ is the azimuth of the $[x_1, x_3]$ symmetry plane in the orthorhombic layers. The values of different parameters are shown by the corresponding colors. The velocity parameters for orthorhombic media are defined in Tsvankin (1997, 2005) and attenuation parameters in Zhu and Tsvankin (2007).

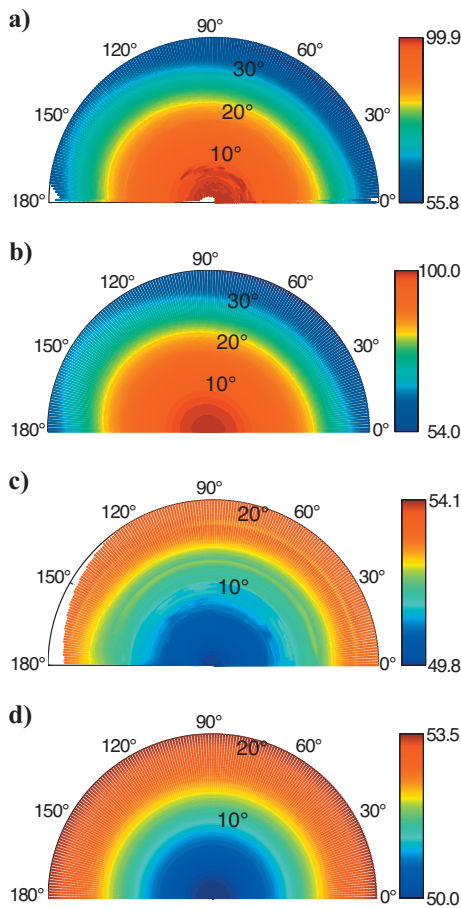


Figure 7. Estimated interval phase attenuation coefficient \mathcal{A} as a function of the phase direction for the (a) second and (c) third layers of the model from Figure 6. The exact $\mathcal{A}|_{\xi=0^\circ}$ in the (b) second and (d) third layers is shown for comparison. All attenuation coefficients are multiplied by 100. The radial axis represents the polar phase angle, and the azimuth is marked on the perimeter.

anisotropy parameters ϵ_Q and δ_Q . In the presence of strong velocity anisotropy, the inversion should be based on the exact solution for $\mathcal{A}|_{\xi=0^\circ}$ obtained from the Christoffel equation.

Note that estimation of the angle θ in an anisotropic target layer generally requires knowledge of the velocity field. Because the influence of attenuation on velocity for a fixed frequency is typically of the second order (Zhu and Tsvankin, 2006), velocity analysis can be performed prior to attenuation processing using the interval travel-time. Anisotropic velocity estimation, however, is often ill posed without a priori information (e.g., the layer thickness). For example, P-wave reflection moveout in a horizontal VTI layer does not constrain either the reflector depth or the group or phase angle for a given source-receiver pair. Still, given typical uncertainties in amplitude measurements, errors in the phase angle are not expected to produce substantial distortions in the attenuation coefficients for moderately anisotropic media.

CONCLUSIONS

We extended velocity-independent layer stripping to amplitude analysis and employed the spectral-ratio method to estimate interval offset- and azimuth-dependent attenuation from reflection data. Although there are no restrictions on heterogeneity and anisotropy in the target horizon, the overburden has to be composed of laterally homogeneous layers with a horizontal symmetry plane (e.g., layers may be orthorhombic). It should be emphasized that our attenuation layer stripping is data driven and does not require knowledge of the overburden velocity and attenuation parameters. In general, the algorithm estimates the average interval group attenuation coefficient along the raypath of a reflected wave. However, for homogeneous target layers, it is possible to reconstruct the normalized phase attenuation coefficient \mathcal{A} for each source-receiver pair. The coefficient \mathcal{A} represents a measure of intrinsic attenuation and can be inverted for the interval attenuation-anisotropy parameters.

Numerical examples for horizontally layered VTI and orthorhombic media confirm that the method yields accurate interval phase attenuation coefficients even for models with uncommonly strong attenuation and substantial velocity and attenuation anisotropy. The algorithm is designed to process isolated overburden and target re-

flections, so the results may be distorted by interference with other events. As with any other layer-stripping technique, the interval attenuation coefficient may become inaccurate for relatively thin layers.

The attenuation coefficient in a reservoir can help to predict the presence and distribution of hydrocarbons (e.g., to distinguish between steam and heat fronts in heavy-oil reservoirs). The 3D version of the method can be used to estimate the azimuthally varying interval attenuation coefficient, which represents a sensitive attribute for fracture characterization and reconstruction of the stress field.

ACKNOWLEDGMENTS

We are grateful to the members of the A(nisotropy)-Team of the Center for Wave Phenomena (CWP), Colorado School of Mines, for helpful discussions. Support for this work was provided by the Consortium Project on Seismic Inverse Methods for Complex Structures at CWP and by the Petroleum Research Fund of the American Chemical Society. The reviews by assistant editor Johan Robertsson and three other reviewers helped to improve the paper.

REFERENCES

- Batzle, M. L., D.-H. Han, and R. Hofmann, 2006, Fluid mobility and frequency-dependent seismic velocity — Direct measurements: *Geophysics*, **71**, no. 1, N1–N9.
- Behura, J., M. Batzle, and R. Hofmann, 2006, Shear properties of oil shales: 76th Annual International Meeting, SEG, Expanded Abstracts, 1973–1977.
- Behura, J., M. Batzle, R. Hofmann, and J. Dorgan, 2007, Heavy oils: Their shear story: *Geophysics*, **72**, E175–E183.
- Behura, J., and I. Tsvankin, 2009, Role of the inhomogeneity angle in anisotropic attenuation analysis: *Geophysics*, **74**, no 5, WB177–WB191.
- Dasgupta, R., and R. A. Clark, 1998, Estimation of Q from surface seismic reflection data: *Geophysics*, **63**, 2120–2128.
- Dewangan, P., and I. Tsvankin, 2006, Velocity-independent layer stripping of PP and PS reflection traveltimes: *Geophysics*, **71**, no. 4, U59–U65.
- Ganley, D. C., and E. R. Kanasewich, 1980, Measurement of absorption and dispersion from check shot surveys: *Journal of Geophysical Research*, **85**, 5219–5226.
- Hosten, B., M. Deschamps, and B. R. Tittmann, 1987, Inhomogeneous wave generation and propagation in lossy anisotropic solids — Application to the characterization of viscoelastic composite materials: *Journal of the Acoustical Society of America*, **82**, 1763–1770.
- Liu, E., M. Chapman, I. Varela, X. Li, J. H. Queen, and H. Lynn, 2007, Velocity and attenuation anisotropy: Implication of seismic fracture characterizations: *Leading Edge*, **26**, 1170–1174.
- Maultzsch, S., M. Chapman, E. Liu, and X. Li, 2007, Modelling and analysis of attenuation anisotropy in multi-azimuth VSP data from the Clair field: *Geophysical Prospecting*, **55**, 627–642.
- Prasad, M., and A. Nur, 2003, Velocity and attenuation anisotropy in reservoir rocks: 73rd Annual International Meeting, SEG, Expanded Abstracts, 1652–1655.
- Schmidt, H., and G. Tango, 1986, Efficient global matrix approach to the computation of synthetic seismograms: *Geophysical Journal of the Royal Astronomical Society*, **84**, 331–359.
- Tao G., and M. S. King, 1990, Shear-wave velocity and Q anisotropy in rocks: A laboratory study: *International Journal of Rock Mechanics and Mining Sciences & Geomechanics Abstracts*, **27**, 353–361.
- Thomsen, L., 1986, Weak elastic anisotropy: *Geophysics*, **51**, 1954–1966.
- Tsvankin, I., 1997, Anisotropic parameters and P-wave velocity for orthorhombic media: *Geophysics*, **62**, 1292–1309.
- , 2005, Seismic signatures and analysis of reflection data in anisotropic media, 2: Elsevier Science.
- Vasconcelos, I., and E. Jenner, 2005, Estimation of azimuthally varying attenuation from wide-azimuth P-wave data: SEG, Expanded Abstracts, **24**, 123–126.
- Wang, X., and I. Tsvankin, 2009, Interval anisotropic parameter estimation using velocity-independent layer stripping: *Geophysics*, **74**, no 5, WB117.
- Winkler, K. W., and A. Nur, 1982, Seismic attenuation: Effects of pore fluids and frictional-sliding: *Geophysics*, **47**, 1–15.
- Zhu, Y., 2006, Seismic wave propagation in attenuative anisotropic media: Ph.D. thesis, Colorado School of Mines.
- Zhu, Y., and I. Tsvankin, 2006, Plane-wave propagation in attenuative transversely isotropic media: *Geophysics*, **71**, no. 2, T17–T30.
- , 2007, Plane-wave attenuation anisotropy in orthorhombic media: *Geophysics*, **72**, no. 1, D9–D19.
- Zhu, Y., I. Tsvankin, P. Dewangan, and K. van Wijk, 2007a, Physical modeling and analysis of P-wave attenuation anisotropy in transversely isotropic media: *Geophysics*, **72**, no. 1, D1–D7.
- Zhu, Y., I. Tsvankin, and I. Vasconcelos, 2007b, Effective attenuation anisotropy of thin-layered media: *Geophysics*, **72**, no 5, D93–D106.